European Journal of Neuroscience, Vol. 25, pp. 2081–2092, 2007 doi:10.1111/j.1460-9568.2007.05463.x

Functional presynaptic HCN channels in the rat globus pallidus

Justin Boyes,[1,2] J. Paul Bolam,[2] Ryuichi Shigemoto[3] and Ian M. Stanford[1]
[1]School of Life and Health Sciences, Aston University, Aston Triangle, Birmingham, B4 7ET, UK
[2]MRC Anatomical Neuropharmacology Unit, University of Oxford, Mansfield Road, Oxford, OX1 3TH, UK
[3]Division of Cerebral Structure, National Institute for Physiological Sciences, Myodaiji, Okazaki 444–8585, Japan

Keywords: basal ganglia, GABA, hyperpolarization-activated cation channel, pre-embedding immunogold, ZD7288

Abstract

Hyperpolarization-activated, cyclic nucleotide-gated cation (HCN) channels are expressed postsynaptically in the rodent globus pallidus (GP), where they play several important roles in controlling GP neuronal activity. To further elucidate the role of HCN channels in the GP, immunocytochemical and electrophysiological approaches were used to test the hypothesis that HCN channels are also expressed presynaptically on the local axon collaterals of GP neurons. At the electron microscopic level, immunoperoxidase labelling for HCN1 and HCN2 was localized in GP somata and dendritic processes, myelinated and unmyelinated axons, and axon terminals. One population of labelled terminals formed symmetric synapses with somata and proximal dendrites and were immunoreactive for parvalbumin, consistent with the axon collaterals of GABAergic GP projection neurons. In addition, labelling for HCN2 and, to a lesser degree, HCN1 was observed in axon terminals that formed asymmetric synapses and were immunoreactive for the vesicular glutamate transporter 2. Immunogold labelling demonstrated that HCN1 and HCN2 were located predominantly at extrasynaptic sites along the plasma membrane of both types of terminal. To determine the function of presynaptic HCN channels in the GP, we performed whole-cell recordings from GP neurons *in vitro*. Bath application of the HCN channel blocker ZD7288 resulted in an increase in the frequency of mIPSCs but had no effect on their amplitude, implying that HCN channels tonically regulate the release of GABA. Their presence, and predicted role in modulating transmitter release, represents a hitherto unidentified mechanism whereby HCN channels influence the activity of GP neurons.

Introduction

The rodent globus pallidus (GP; and its primate equivalent, the external segment of the GP) plays a central role in basal ganglia function and dysfunction (Levy *et al*., 1997; Obeso *et al*., 2006). It is composed of a network of GABAergic projection neurons which provide the main inhibitory input to the subthalamic nucleus (STN; Smith *et al*., 1990a). In addition, GP neurons send projections to the basal ganglia output nuclei and to the striatum (Kita & Kitai, 1994; Bevan *et al*., 1998; Kita *et al*., 1999; Sato *et al*., 2000). By virtue of this extensive connectivity, individual GP neurons are in a powerful position to influence the activity of neurons at every level of the basal ganglia.

GP neurons recorded *in vitro* are autonomously active and discharge in a highly regular manner (Kita & Kitai, 1991; Nambu & Llinás, 1997; Cooper & Stanford, 2000; Stanford, 2003; Chan *et al*., 2004). In awake or anaesthetized animals, however, GP neuronal firing is more heterogeneous (DeLong, 1971; Magill *et al*., 2000; Raz *et al*., 2000), indicating that synaptic inputs are critical for the expression of behaviourally relevant patterns of GP activity *in vivo*. The major afferents to GP neurons are a GABAergic projection from the striatum and a glutamatergic projection from the STN (Smith *et al*., 1998). In addition, GP neurons receive input from the local axon collaterals of neighbouring neurons (Kita & Kitai, 1994; Bevan *et al*., 1998; Sadek *et al*., 2005). It is predicted that the interplay between glutamatergic and GABAergic inputs are a major determinant of the spontaneous activity of GP neurons (Kita *et al*., 2004). Furthermore, in network models, alterations in the relative strengths of these inputs leads to aberrant rhythmic patterns of activity (Terman *et al*., 2002) that resemble those seen in the GP in experimental models of Parkinson's disease (Filion & Tremblay, 1991; Raz *et al*., 2000). Consequently, it is of critical importance to elucidate the mechanisms modulating synaptic transmission and therefore neuronal activity in the GP (see Chen & Yung, 2004; Chan *et al*., 2005).

The depolarizing current carried by hyperpolarization-activated, cyclic nucleotide-gated cation (HCN) channels, termed I_h, is observed in the majority of GP neurons (Cooper & Stanford, 2000; Chan *et al*., 2004), where it has been shown, *in vitro*, to contribute to the resting membrane potential and to the rate and regularity of action potential firing (Chan *et al*., 2004). In addition to these postsynaptic functions, HCN channels may also be involved in the presynaptic regulation of synaptic transmission in the GP, as has been proposed in several other brain regions (for review, see Robinson & Siegelbaum, 2003). In this study, we examined the subcellular localization of the HCN channel subunits HCN1 and HCN2 at the electron microscopic level. Specifically, we tested the hypothesis that HCN channels are expressed on the local axon collaterals of GP neurons. In addition, we investigated the possible role of presynaptic HCN channels in the modulation of inhibitory synaptic transmission in the GP.

Correspondence: Dr. I.M. Stanford, [1]School of Life and Health Sciences, Aston University, as above.
E-mail: i.m.stanford@aston.ac.uk

Received 30 November 2006, revised 19 January 2007, accepted 5 February 2007

Materials and methods

All procedures involving animals were performed in accordance with the United Kingdom Animals (Scientific Procedures) Act 1986. All efforts were made to minimize the number of animals used. For immunocytochemical studies, nine adult male Sprague–Dawley rats (250–350 g; Charles River, Margate, UK) were deeply anaesthetized with ketamine (Ketaset; 70 mg/kg; Willows Francis Veterinary, Crawley, UK) and medetomidine (Domitor; 0.5 mg/kg; Pfizer, Sandwich, UK) and perfused via the ascending aorta with phosphate-buffered saline (PBS; 0.01 M phosphate, pH 7.4) followed by 300 mL of fixative solution containing 4% paraformaldehyde and 0.05% glutaraldehyde in 0.1 M phosphate buffer (PB; pH 7.4). An additional two rats aged postnatal day (P)14 were perfused with a smaller volume of the same fixative solution. After postperfusion with PBS, brains were removed and stored in PBS at 4 °C. Coronal or sagittal sections were cut on a vibratome at 50 μm for light microscopy or 65 μm for electron microscopy.

Primary antibodies

We used polyclonal antibodies raised in guinea pig against the C-terminus of HCN1 (N12) and HCN2 (N21). The production and characterization of these antibodies has been described elsewhere (Lörincz *et al*., 2002; Notomi & Shigemoto, 2004). All other primary antibodies used were purchased from commercial sources: rabbit anti-HCN1 (Alomone Laboratories, Jerusalem, Israel; for characterization, see Lörincz *et al*., 2002), mouse anti-parvalbumin (Sigma–Aldrich, Gillingham, UK), rabbit anti-vesicular glutamate transporter 2 (VGLUT2; Synaptic Systems, Göttingen, Germany).

Immunocytochemistry for electron microscopy

The procedures used for pre-embedding immunolabelling were similar to those described previously (Chen *et al*., 2004; Lacey *et al*., 2005). Sections for electron microscopy were freeze–thawed, washed in PBS and then incubated in blocking solution containing 10% normal goat serum (NGS; Vector Laboratories, Peterborough, UK) in PBS for 2 h. All subsequent antibody incubations were carried out in PBS containing 2% NGS and sections were washed several times between steps. For single immunolabelling of HCN channel subunits, sections were incubated in guinea pig primary antibodies at final concentrations of 1.5–2.0 μg/mL (HCN1) and 0.5 μg/mL (HCN2), for a minimum of 48 h at 4 °C. Sections for immunoperoxidase labelling were incubated in biotinylated anti-guinea pig IgG (1 : 200; Vector) for 2–3 h, followed by 2 h in avidin–biotin–peroxidase complex (ABC; 1 : 100 in PBS; Vector), at room temperature. After equilibrating in Tris buffer (0.05 M, pH 7.6), the peroxidase was revealed by incubating the sections in 0.025% diaminobenzidine (DAB; Sigma–Aldrich) in the presence of 0.01% H_2O_2 for 6–8 min. For immunogold labelling, sections were incubated in anti-guinea pig IgG (Fab fragment) coupled to 1.4-nm gold particles (1 : 100; Nanoprobes, Yaphank, NY, USA) for 3–4 h at room temperature. The gold particles were then silver-enhanced using the HQ Silver kit (Nanoprobes).

In double-immunolabelling experiments, immunogold labelling and silver enhancement were performed before immunoperoxidase labelling to prevent the nonspecific deposition of silver on the peroxidase reaction product. Sections were incubated in guinea pig anti-HCN2 plus rabbit anti-HCN1 (1 : 400), mouse anti-parvalbumin (1 : 2000), or rabbit anti-VGLUT2 (1 : 2000). The sections were then incubated in gold-conjugated anti-guinea pig IgG (1 : 100) and either biotinylated anti-mouse or biotinylated anti-rabbit IgG (1 : 200; Vector), overnight at 4 °C. Gold labelling was revealed by silver enhancement using the HQ Silver kit and peroxidase labelling by incubation in ABC followed by a peroxidase reaction using DAB, as described above.

All sections were postfixed in 1% osmium tetroxide (Oxkem, Reading, UK) in PB for < 10 min (for immunogold- and double-labelled sections) or 25 min (for immunoperoxidase-labelled sections), dehydrated through a graded series of ethanol dilutions, with 1% uranyl acetate (TAAB, Aldermaston, UK) added to the 70% solution, and embedded in resin (Durcupan ACM Fluka; Sigma–Aldrich) on glass microscope slides. Following light microscopic examination, areas of the dorsolateral GP were removed and glued to blank cylinders of resin. Serial ultrathin sections (∼ 60 nm) were cut on an ultramicrotome and collected on pioloform-coated, single-slot copper grids. Ultrathin sections were then contrasted with lead citrate for 2–3 min and analysed in a Philips CM100 electron microscope.

Immunocytochemistry for light microscopy

Sections were processed for immunoperoxidase labelling of HCN1 and HCN2 in an identical manner to those for electron microscopy, except that the freeze–thawing step was omitted and 0.3% Triton X-100 was included in the antibody solutions. Following visualization by the peroxidase reaction, the sections were dehydrated and mounted on slides.

Controls

The specificity of the HCN2 antibody was tested on brain tissue from HCN2-null mice (kindly provided by Dr A. Ludwig, Institut für Pharmakologie, Technische Universität München, Germany). Immunolabelling was absent in sections from mice lacking HCN2 but was present in sections from wild-type littermates (Fig. 1). In addition, the method specificity was confirmed by the lack of immunolabelling in sections that were processed for electron microscopy without the primary antibody. To control for possible cross-reactivity of the secondary antibodies in double-labelling experiments, sections were processed in parallel through the same immunocytochemical protocol except that only one primary antibody was included. No evidence of cross-reactivity was apparent under these conditions.

Quantitative analyses

Electron micrographs were captured digitally using a Gatan Ultrascan 1000 CCD digital camera with DigitalMicrograph software (Gatan UK, Abingdon, UK). The characterization of axon terminals expressing presynaptic HCN channels was performed on immunoperoxidase-labelled tissue from three animals each for HCN1 and HCN2. Sections were scanned and labelled terminals were digitally imaged for off-line analysis. The cross-sectional area of labelled terminals was measured using the public domain image analysis software Image J (NIH, USA). The structures postsynaptic to labelled terminals were categorized as cell bodies, large dendrites (minimum cross-sectional diameter > 1.5 μm) or small dendrites (minimum cross-sectional diameter < 1.5 μm).

Analysis of the subcellular distribution of HCN channels was carried out in tissue that was double-labelled for HCN2 and either parvalbumin or VGLUT2. Sections were scanned and double-labelled terminals were digitally imaged. In Image J, the location of immunogold particles relative to synaptic sites was calculated by measuring the distance from the centre of each membrane-bound gold particle to

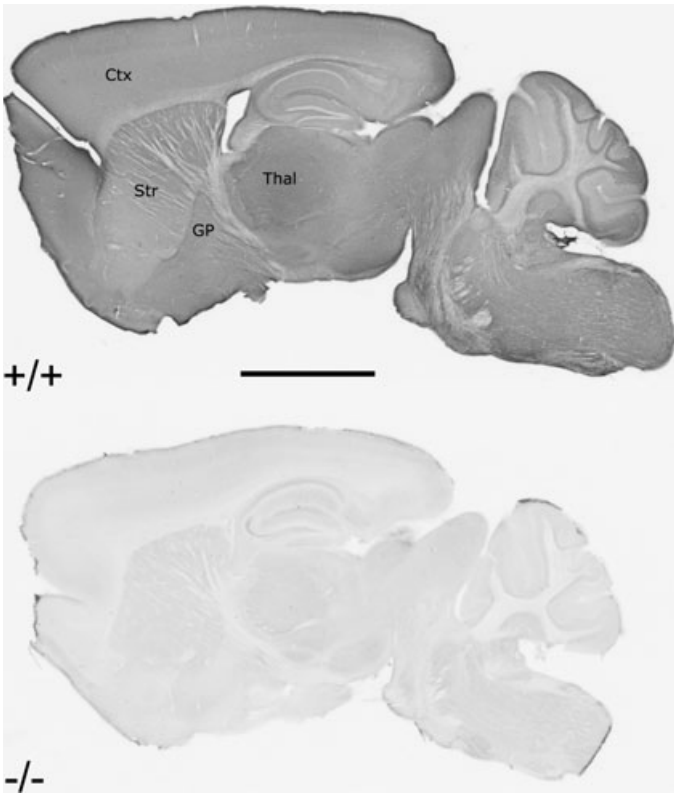

FIG. 1. Immunoreactivity for HCN2 in homozygous wild-type (+/+) and HCN2-null (–/–) mice. Note the lack of immunolabelling in the brain section from the $HCN2^{-/-}$ mice, confirming the specificity of the antibody to HCN2. Ctx, cerebral cortex; GP, globus pallidus; Thal, thalamus; Str, striatum. Scale bar, 2.5 mm.

the closest edge of the presynaptic membrane specialization. To take into account the size of the primary and secondary antibodies, and of the intracellular epitope of the HCN channel subunits, a gold particle was considered to be membrane-bound if its centre was within 25 nm of the plasma membrane. The number of gold particles was expressed as a relative frequency in bins corresponding to 60-nm-wide subdivisions of the axon terminal membrane.

Electrophysiological recording

Recordings were made in brain slices from male rats aged P14–18. Animals were anaesthetized with fluorothane and decapitated. Brains were removed and placed in ice-cold artificial cerebrospinal fluid (aCSF) containing (in mM): sucrose, 206; KCl, 2.5; $MgCl_2$, 1; $CaCl_2$, 2; NaH_2PO_4, 1.25; and glucose, 10 (buffered to pH 7.4 with 26 mM $NaHCO_3$). Hemicoronal slices (300 μm) containing the GP were cut using a DTK-1000 Microslicer (Dosaka, Japan) and maintained at room temperature in a holding chamber filled with aCSF containing (in mM): NaCl, 126; KCl, 2.5; $MgCl_2$, 1.3; $CaCl_2$, 2.4; NaH_2PO_4, 1.2; and glucose, 10 (buffered to pH 7.4 with 26 mM $NaHCO_3$). The slices were then transferred to the recording chamber where they were continuously superfused with the same aCSF (2–3 mL/min) at 32–34 °C. All aCSF was saturated with 95% O_2–5% CO_2.

Individual GP neurons were visualized by differential interference contrast infrared microscopy using an Olympus BX51WI microscope with a CCD camera (KP-M1; Hitachi, Japan). Whole-cell patch-clamp recordings were made using borosilicate glass pipettes (3–6 MΩ resistance) filled with a high-Cl^- intracellular solution consisting of (in mM): KCl, 125; NaCl, 10; $CaCl_2$, 1; $MgCl_2$, 2; BAPTA, 10; HEPES, 10; GTP, 0.3; Mg-ATP, 2; and QX-314, 5 (adjusted to pH 7.3 with KOH). QX-314 was included to eliminate Na^+-dependent action potentials and to block postsynaptic HCN channels in the GP neurons from which recordings were made (Perkins & Wong, 1995). In addition, 5 mM biocytin was added to the pipette solution to enable *post hoc* identification of the recorded neurons. Membrane currents were recorded in cells voltage-clamped at −80 mV using an Axopatch 200B patch-clamp amplifier (Axon Instruments, Foster City, CA, USA). Series resistance was not compensated, but was monitored throughout by measuring the capacitance currents generated by 5-mV hyperpolarizing steps. Cells were rejected from the analysis if the series resistance changed by > 20% during the course of the recording. GABAergic synaptic transmission was isolated pharmacologically by adding the glutamate receptor antagonists 6-cyano-7-nitroquinoxaline-2,3-dione (CNQX; 10 μM) and DL-2-amino-5-phosphonopentanoic acid (DL-AP5; 50 μM; both Sigma–Aldrich) to the aCSF. Miniature inhibitory postsynaptic currents (mIPSCs) were recorded in the presence of tetrodotoxin (TTX; 1 μM; Sigma–Aldrich). HCN channels were blocked by superfusion with ZD7288 (50 μM; Tocris, Bristol, UK) for a minimum of 15 min.

Histology

Following electrophysiological recording, slices were left in the recording chamber for at least 45 min and then fixed by immersion in 4% paraformaldehyde in PB (pH 7.4) at 4 °C. After at least 24 h in fixative, slices were processed to reveal the biocytin-filled cells using the ABC method. Briefly, slices were incubated in ABC overnight at 4 °C and then peroxidase activity was revealed using DAB as the chromogen. The slices were then dehydrated and mounted on slides for light-microscopic evaluation.

Data analysis

Data were acquired using Signal software (Cambridge Electronic Design, Cambridge, UK) and analysed using MiniAnalysis (Synaptosoft, Decatur, GA, USA). mIPSCs were automatically detected using an amplitude threshold selected on a cell-to-cell basis. Detected events were excluded from the analyses if the rise time exceeded the decay time. For each neuron, the mean interevent interval and amplitude of mIPSCs were calculated from 100 events immediately preceding drug application and following 10 min bath application of ZD7288. Statistical comparisons were made using a paired *t*-test, with significance accepted at $P < 0.05$. Changes in the cumulative interevent interval and amplitude distributions of mIPSCs were analysed using the Kolmogorov–Smirnov test, which estimates the probability that two distributions are similar. For this analysis, a more conservative probability level of $P < 0.01$ was selected for statistical significance. All numerical data are expressed as mean ± SEM unless otherwise stated.

Results

Cellular distribution of HCN1 and HCN2: light microscopy

The regional distributions of HCN1 and HCN2 at the light-microscopic level were similar to previous descriptions (Chan *et al*., 2004; Notomi & Shigemoto, 2004). Thus, the GP was weakly

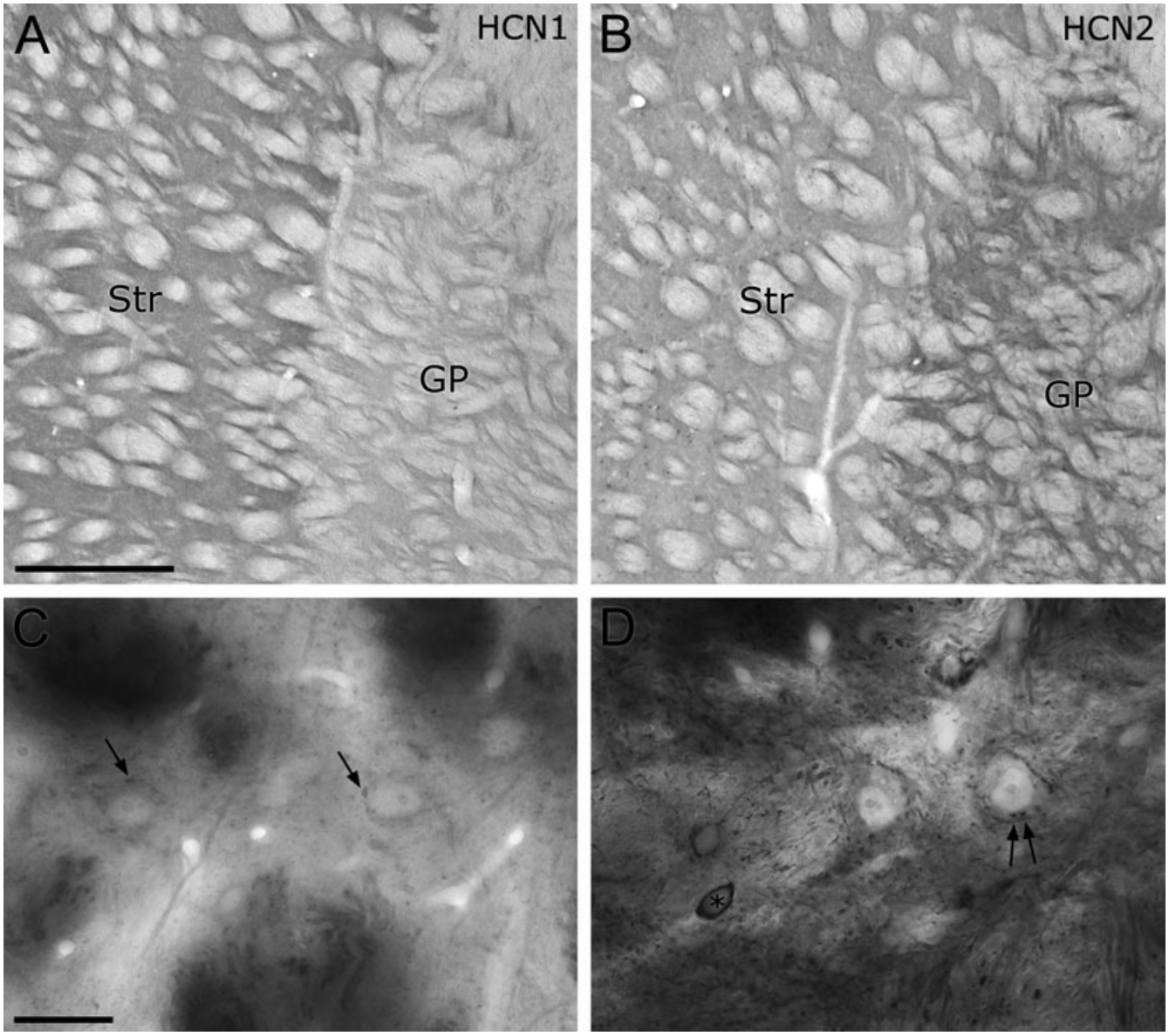

FIG. 2. Patterns of immunoreactivity for HCN channel subunits in the GP. (A and B) Light micrographs of (A) HCN1 and (B) HCN2 immunoperoxidase labelling showing the predominance of immunoreactivity for HCN2 in the GP. In contrast, HCN1 immunoreactivity is stronger in the striatum (Str). (C and D) Higher magnification images showing immunoperoxidase labelling for HCN1 and HCN2 in tissue prepared for electron microscopy. Labelling for both subunits is largely restricted to the neuropil, including punctate structures apposed to GP somata (arrows). In addition, strong labelling for HCN2, but not HCN1, is present in glial cells (asterisk in D). Scale bars, 0.5 mm (A and B), 25 μm (C and D).

immunoreactive for HCN1 (Fig. 2A). In contrast, intense immunoreactivity for HCN2 was observed throughout the GP (Fig. 2B). Moderate immunoreactivity for HCN1 and HCN2 was also present in the striatum, where the strength of labelling for the two subunits was similar (Fig. 2A and B). When viewed at higher magnification, immunolabelling for both subunits in the GP was largely restricted to neuropil elements (Fig. 2C and D). A prominent feature of this was the labelling of presumed axon terminals that were closely apposed to unlabelled GP neuronal cell bodies and proximal dendrites (Fig. 2C and D). In addition, small cells with thin processes were strongly immunoreactive for HCN2 but not HCN1 (Fig. 2D). These HCN2-positive cells were observed in most brain regions and have been identified as a subtype of oligodendrocyte (Notomi & Shigemoto, 2004).

Subcellular localization of HCN1 and HCN2: electron microscopy

Immunoperoxidase

At the electron-microscopic level, immunoperoxidase labelling for HCN1 and HCN2 was observed in cell bodies and dendritic shafts of GP neurons (Fig. 3A and B). However, the most prominent labelling for both HCN channel subunits was detected in presynaptic structures (Fig. 3C–G). At least two populations of HCN-labelled terminals were observed. The first consisted of terminals with a large cross-sectional area (HCN1, 0.83 ± 0.30 μm^2, $n = 72$; HCN2, 0.89 ± 0.32 μm^2, $n = 87$; mean ± SD) which typically contained several mitochondria and often possessed multiple synaptic release sites (Fig. 3C–E). These terminals formed symmetric synapses with cell bodies (HCN1, 44.4%;

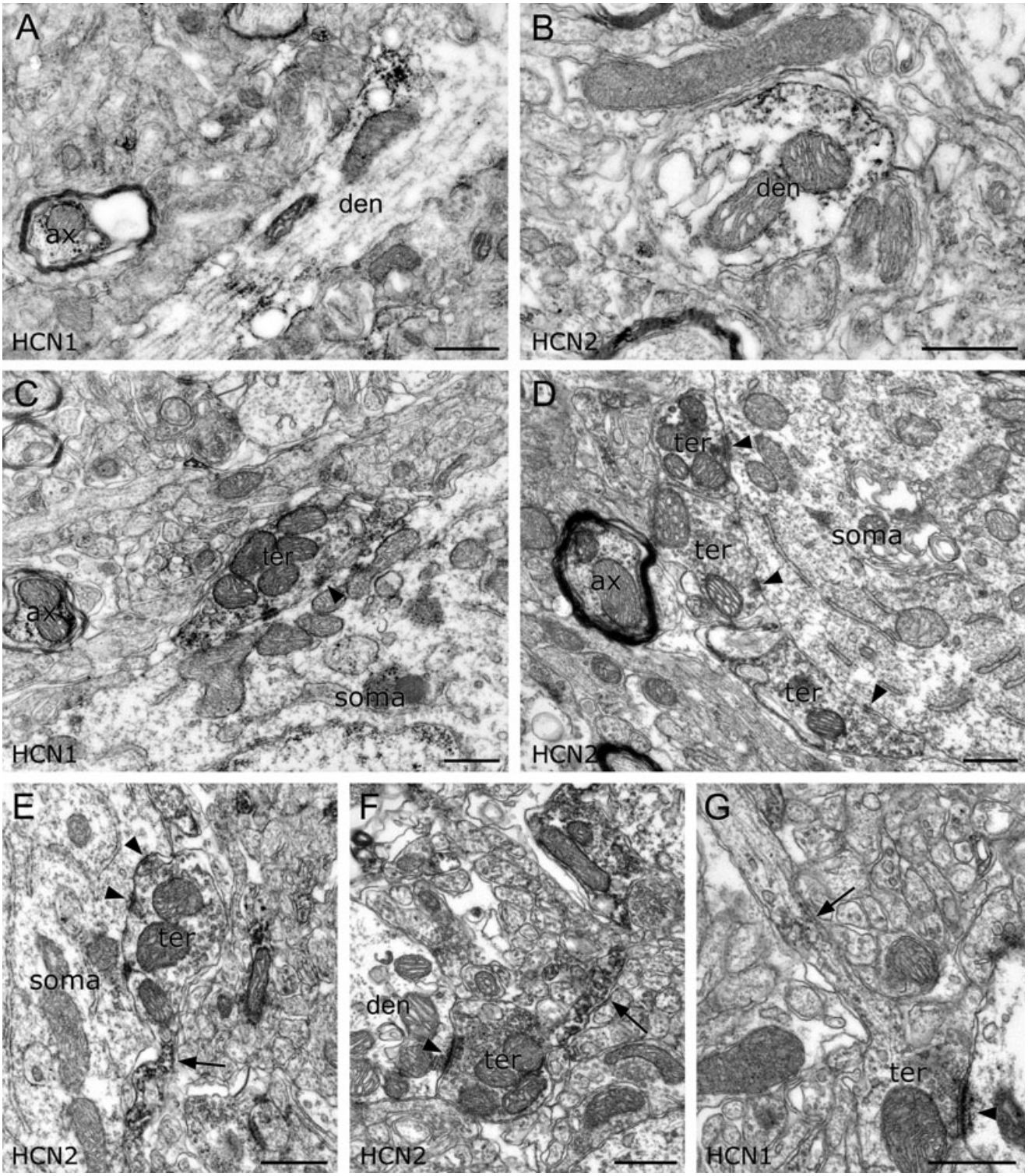

FIG. 3. Immunoperoxidase labelling for HCN1 and HCN2 in the GP. (A and B) Labelling for HCN1 and HCN2 in dendrites (den) in the GP. In A, a myelinated axon (ax) is also labelled for HCN1. (C and D) Labelling for (C) HCN1 and (D) HCN2 in terminals (ter) forming symmetric synapses (arrowheads) with GP somata. The morphological features of these terminals and the perisomatic pattern of innervation are typical of the terminals of GP axon collaterals. Note the myelinated axons labelled for HCN1 and HCN2. (E) An HCN2-labelled axon terminal forming a symmetric synapse (arrowhead) illustrating strong labelling in the preterminal portion of the axon (arrow). (F) HCN2 labelling in an axon terminal forming an asymmetric synapse (arrowhead) with a dendrite (den). Note the strong labelling in the preterminal portion of the axon (arrow). The same axon also gives rise to a second HCN2-positive terminal that does not form a synapse in this section. (G) HCN1 labelling (arrow) in an axon that gives rise to a terminal forming an asymmetric synapse (arrowhead) with a dendrite. Scale bars, 0.5 μm.

HCN2, 45.4%), large dendrites (HCN1, 30.6%; HCN2, 26.7%) and small dendrites (HCN1, 25.0%; HCN2, 27.9%). These characteristics are consistent with those described for terminals of the recurrent axon collaterals of GP projection neurons (Sadek *et al*., 2005), as well as for GP axon terminals in other basal ganglia nuclei (see Smith *et al*., 1998). The majority of terminals forming symmetric synapses with GP

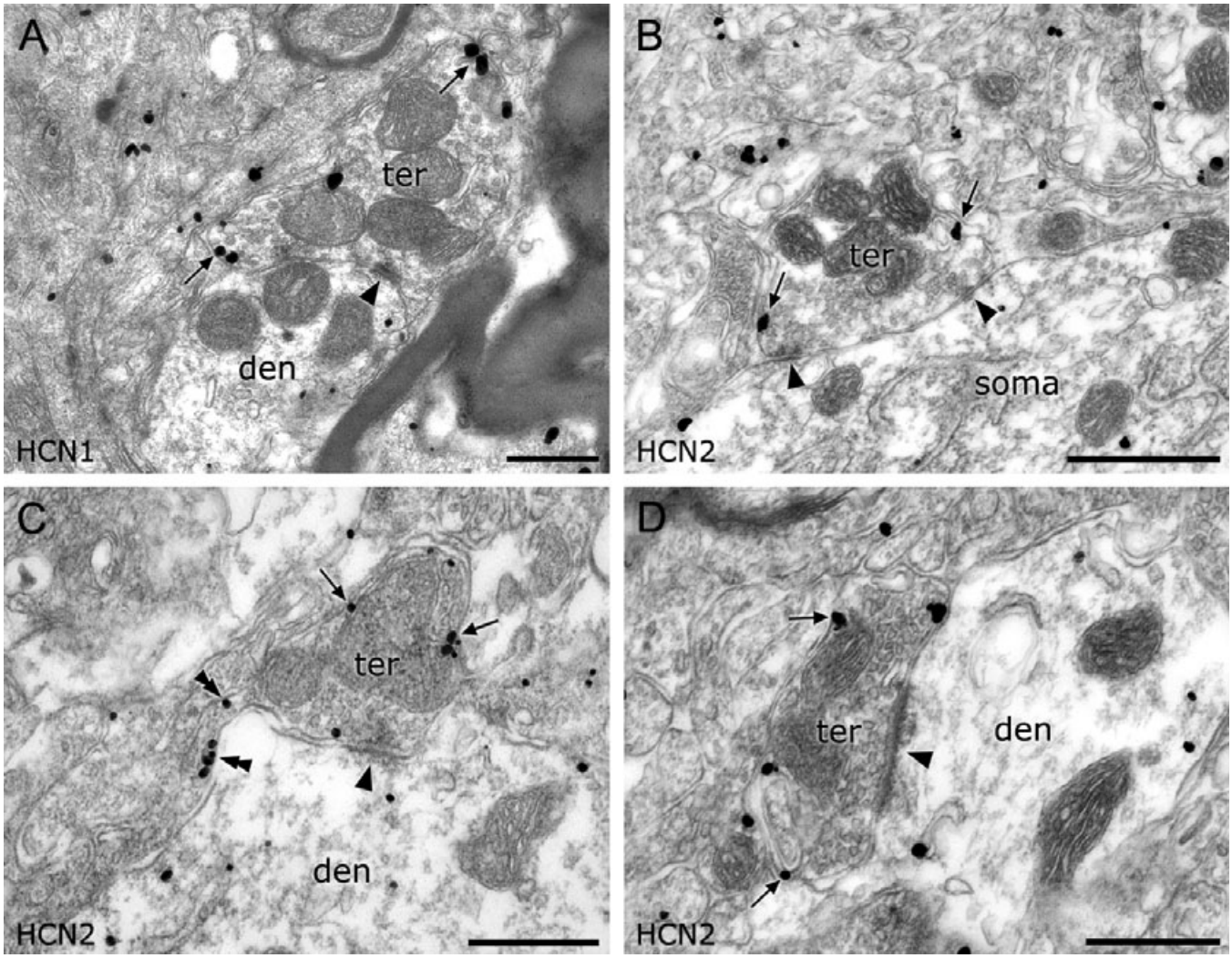

FIG. 4. Immunogold labelling for HCN1 and HCN2 in axon terminals in the GP. (A and B) Labelling for HCN1 and HCN2 on the plasma membrane in GP-like axon terminals (ter) forming symmetric synapses (arrowheads) with a dendrite (den) and soma, respectively. Note the extrasynaptic location of the gold particles (some indicated by arrows). (C and D) Labelling for HCN2 in axon terminals forming asymmetric synapses (arrowheads) with dendrites. Gold particles (some indicated by arrows) are located at extrasynaptic sites on the terminal membrane. In C, gold particles are also present in the preterminal axon (double arrowheads). Scale bars, 0.5 μm.

dendrites possessed the morphological features of striatopallidal terminals and were unlabelled for either subunit. Strong immunolabelling for HCN2 was observed in axon terminals establishing asymmetric synapses (Fig. 3F). These were smaller than the putative GP axon collateral terminals (0.53 ± 0.19 μm^2, $n = 132$) and innervated small dendrites (87.9%) more frequently than cell bodies (0.7%) or large dendrites (11.4%), consistent with terminals derived from the STN (Smith *et al.*, 1998). Labelling for HCN1 was considerably less intense in terminals forming asymmetric synapses (Fig. 3G). It is unlikely that this was due to differences in the quality and/or affinity of the antibodies as the intensity of labelling of putative GP axon collateral terminals in the same sections was similar for HCN1 and HCN2.

In addition to the labelling in axon terminals, peroxidase reaction product for both HCN1 and HCN2 was observed in many large myelinated axons and small unmyelinated axons including, when visible, the preterminal portion of axons (Fig. 3A and C–G). When labelled axon terminals could be followed to their preterminal axons, they were often more strongly labelled than the terminals (Fig. 3E–G, arrows).

Immunogold

To define the subcellular distribution of HCN channels in axons and terminals in the GP, we performed pre-embedding immunogold labelling for HCN1 and HCN2. Consistent with the intracellular nature of the epitopes against which the antibodies were raised, silver-enhanced gold particles were associated with the cytoplasmic surface of the plasma membrane in both presynaptic and postsynaptic structures (Figs 4 and 5A–C). In addition, gold particles were associated with intracellular membranes, including endoplasmic reticulum (Figs 4B–D and 5B and C). In qualitative terms, the strongest labelling was found on the membrane of myelinated axons. Labelled axons were often located within the large bundles of axons that course through the GP, but were more commonly found in isolation in the surrounding neuropil. Immunogold labelling was also prominent in unmyelinated axons and in axon terminals. Gold particles were associated with the axonal plasma membrane of labelled terminals (Fig. 4) and preterminal axons (Fig. 4C). Consistent with the immunoperoxidase data, labelling for HCN1 and HCN2 was localized in putative GP axon collateral terminals forming

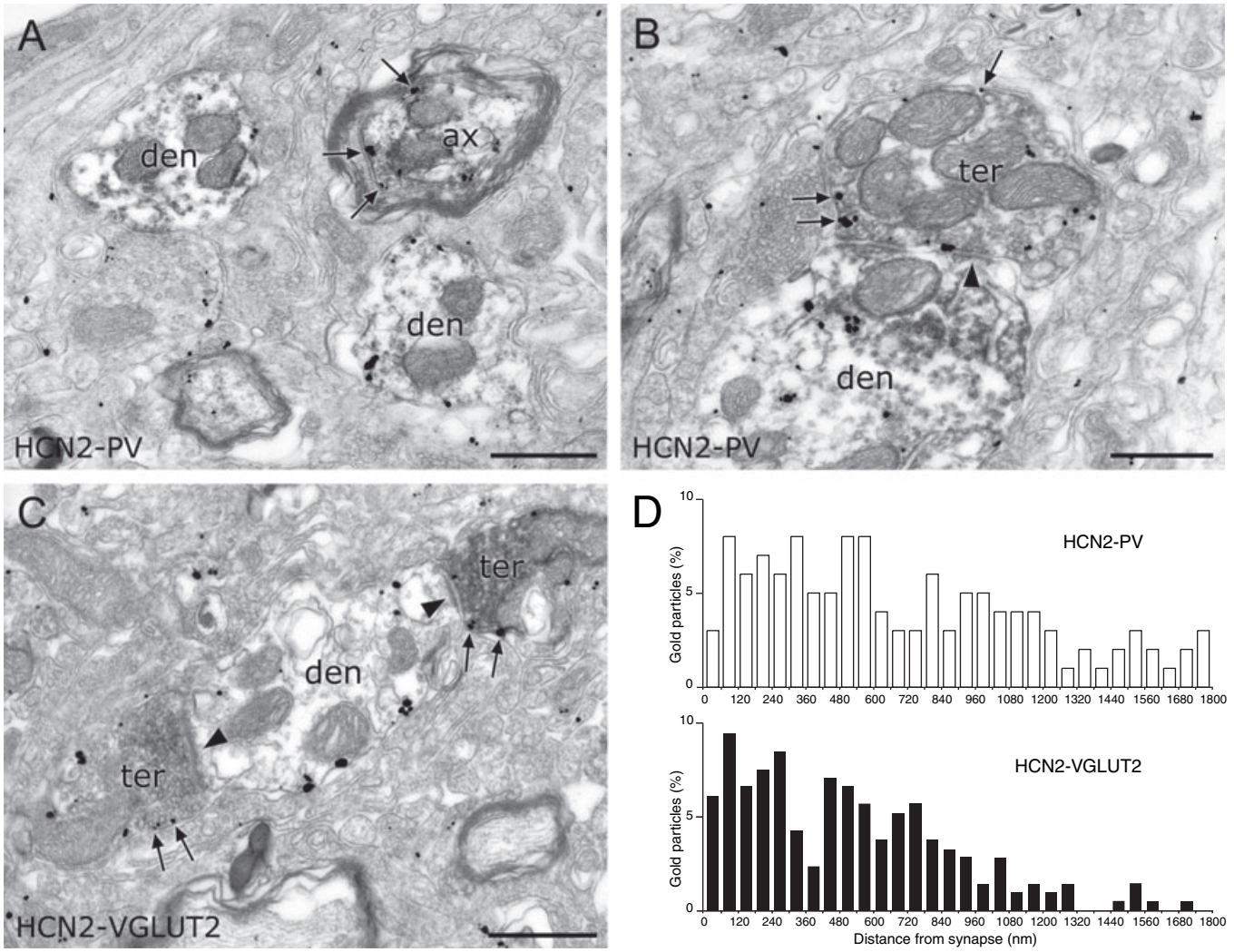

FIG. 5. Co-localization of HCN2 with parvalbumin and VGLUT2 in axons and axon terminals in the GP. (A) Immunogold labelling for HCN2 (arrows) in a PV-labelled myelinated axon (peroxidase reaction product; ax). Two adjacent PV-labelled dendrites (den) are also labelled for HCN2. (B) Labelling for HCN2 at extrasynaptic sites on the plasma membrane (arrows) of a PV-positive axon terminal (ter). The terminal forms a symmetric synapse (arrowhead) with a dendrite that is also labelled for both PV and HCN2. (C) Labelling for HCN2 in two VGLUT2-positive terminals forming asymmetric synapses (arrowheads) with an HNC2-positive dendrite. Gold particles are localized mostly at extrasynaptic sites on both the axonal (arrows) and dendritic membranes. (D) Histograms showing the spatial distribution of immunogold particles for HCN2 on the plasma membrane of axon terminals immunopositive for PV ($n = 128$) and VGLUT2 ($n = 213$). The number of gold particles is expressed as a relative frequency in bins corresponding to 60-nm-wide subdivisions of the axon terminal membrane. Scale bars, 0.5 μm.

symmetric synapses with cell bodies and dendrites (Fig. 4A and B). In addition, labelling for HCN2 was detected in axon terminals forming asymmetric synapses with dendrites (Fig. 4C and D).

To gain further insight into the nature of HCN-immunoreactive axons and axon terminals, we carried out double immunolabelling for HCN2 and parvalbumin, a calcium-binding protein present in about two-thirds of GP neurons (Kita, 1994). These experiments revealed that many parvalbumin-immunoreactive axons and axon terminals were also immunogold-labelled for HCN2 (Fig. 5A and B). The double-labelled terminals formed symmetric synapses with GP cell bodies and large dendrites. In addition, we double labelled for VGLUT2, a marker of glutamatergic terminals (Fremeau *et al*., 2004). In agreement with our previous study, the majority of terminals forming asymmetric synapses in the GP were strongly immunoreactive for VGLUT2 (Chen *et al*., 2004), and many of these were immunogold-labelled for HCN2 (Fig. 5C). In both single- and double-labelled terminals, gold particles were located almost exclusively at extrasynaptic sites along the plasma membrane and only occasionally detected at the presynaptic active zone (Figs 4 and 5B and C). To examine more closely the spatial relationship between HCN channels and neurotransmitter release sites, we quantified the distribution of immunogold labelling in double-labelled terminals. This analysis confirmed that gold particles for HCN2 ($n = 128$) were distributed across the full extent of the plasma membrane in parvalbumin-positive terminals (Fig. 5D). In VGLUT2-positive terminals, gold particles ($n = 213$) were similarly distributed, albeit over a more restricted distance (Fig. 5D), presumably as a result of the smaller size of these terminals.

In most cases, the postsynaptic targets of HCN-labelled terminals were immunoreactive for the particular channel subunit when examined in serial sections. Gold particles in dendrites were localized mainly on the plasma membrane at sites distant from either symmetric or asymmetric synapses (Figs 4 and 5; see also Fig. 6A).

Co-localization of HCN1 and HCN2

The similarity in the patterns of immunolabelling for HCN1 and HCN2 suggested that the two subunits were coexpressed in individual

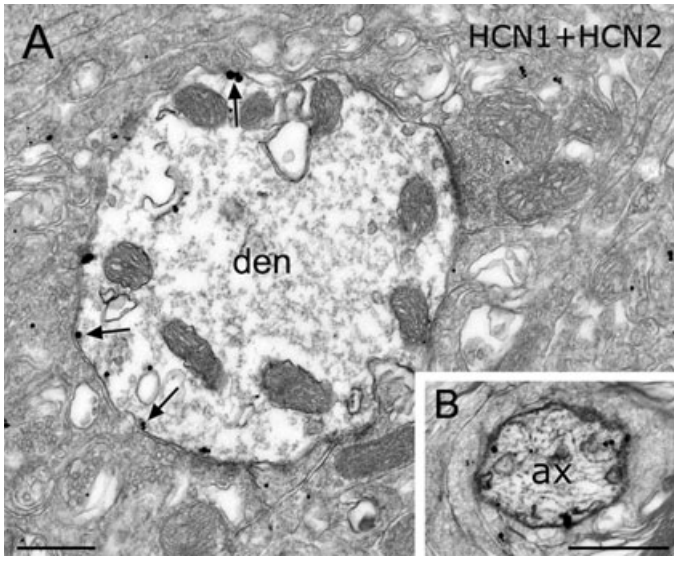

FIG. 6. Co-localization of HCN1 and HCN2 in presynaptic and postsynaptic elements in the GP. Labelling for HCN1 is with immunoperoxidase and for HCN2 with immunogold. (A) Co-localization of HCN1 and HCN2 in a dendrite (den). Although the strength of labelling for HCN1 is diminished when compared with single-labelled tissue, the peroxidase reaction product is visible in the cytoplasm of the dendrite. Gold particles for HNC2 are associated with extrasynaptic sites on the plasma membrane (arrows). (B) Co-localization of HCN1 and HCN2 in a myelinated axon (ax). Scale bars, 0.25 μm (A), 0.5 μm (B).

GP neurons. To directly test this, we performed double immunolabelling for HCN1 and HCN2 using an antibody against HCN1 raised in rabbit. Although the strength of immunoperoxidase labelling for HCN1 was diminished in double-labelled tissue, colocalization of HCN1 and HCN2 was detected in both dendrites and myelinated axons (Fig. 6A and B).

Role of HCN channels in GABA release

To address the possible role of presynaptic HCN channels in modulating GABA release in the GP, we examined the effect of the HCN channel blocker ZD7288 on mIPSCs recorded from GP neurons *in vitro*. Because these experiments were performed in brain slices from juvenile rats (P14–18), we first confirmed the presynaptic expression of HCN channel subunits at this age. At P14, the patterns of immunoperoxidase labelling for HCN1 and HCN2 in putative inhibitory axon terminals closely resembled those observed in adult rats (Fig. 7A).

mIPSCs were recorded from visually identified GP neurons at a holding potential of −80 mV in the presence of 1 μM TTX, 10 μM CNQX and 50 μM DL-AP5 (Fig. 7B). In all experiments, the location of the recorded neurons within the GP was confirmed by light microscopic analysis following histological processing to reveal the biocytin-filled cells (data not shown). Under control conditions, the mean interevent interval of mIPSCs was 1042.7 ± 48.3 ms ($n = 5$). Application of 50 μM ZD7288 resulted in a significant reduction in the mean mIPSC interevent interval, i.e. an increase in mIPSC frequency (Fig. 7B). Thus, the mean interevent interval of mIPSCs measured after 10 min ZD7288 application was 736.4 ± 41.5 ms ($P < 0.05$, paired *t*-test), representing a decrease of ∼30%. In contrast, the mean amplitude of mIPSCs was not significantly changed by ZD7288 (62.9 ± 2.6 vs. 57.8 ± 2.2 pA; $P > 0.05$, paired *t*-test). Analysis of the cumulative probability distribution of the interevent intervals of mIPSCs revealed a significant shift towards shorter intervals following 10 min ZD7288 application ($P < 0.01$, Kolmogorov–Smirnov test), indicating an increase in the frequency of mIPSCs, whereas the distribution of the amplitudes was not altered (Fig. 7C). In an additional two experiments in which glutamate receptor antagonists were not used, ZD7288 also significantly reduced the mean interevent interval of mIPSCs without affecting the mean amplitude (data not shown).

Discussion

HCN channels located postsynaptically on GP neurons play several important roles in controlling their output (Chan *et al*., 2004). In the present study we demonstrate for the first time that HCN channel subunits are also expressed presynaptically in the GP. Our results reveal that HCN channels are located on the terminals of GP axon collaterals and presumed STN terminals. In contrast, no evidence was found for HCN channel subunits on striatopallidal terminals. Their presence at presumed STN and GP axon collateral terminals, and predicted role in modulating GABA (and glutamate) release, represents a hitherto unidentified mechanism whereby HCN channels influence the activity of GP neurons.

Presynaptic HCN channels on inhibitory and excitatory axon terminals

Our results demonstrate that the HCN channel subunits HCN1 and HCN2 are localized on putative inhibitory axon terminals that form symmetric synapses predominantly with GP cell bodies and proximal dendrites. Many of these terminals were immunoreactive for parvalbumin, supporting the notion, based on morphological criteria, that they are derived from the local axon collaterals of GP projection neurons (Kita & Kitai, 1994; Sadek *et al*., 2005). This finding follows recent studies showing HCN1 and HCN2 protein in inhibitory terminals in both the hippocampus (Notomi & Shigemoto, 2004) and cerebellum (Luján *et al*., 2005). The perisomatic innervation by GP axon collateral terminals contrasts with striatopallidal terminals, which represent the large majority (> 80%) of the total synaptic input to GP neurons and which mainly target the dendrites of GP neurons (Smith *et al*., 1998). Terminals with the morphological characteristics of those derived from the striatum were negative for both subunits, indicating that HCN channels are not expressed presynaptically by striatopallidal neurons. Although the absence of labelling for HCN channels on putative striatopallidal terminals may simply reflect a low level of expression on these terminals, our results are consistent with the lack of I_h in striatal spiny projection neurons (Jiang & North, 1991; Kawaguchi, 1993). This poses the question as to the origin of labelling for HCN1 and HCN2 observed in the striatum at the light-microscopic level. To this end, preliminary investigations at the ultrastructural level indicate that HCN1 is localized mainly at presynaptic sites in the striatum, including axonal profiles and terminals resembling pallidostriatal terminals (Bevan *et al*., 1998; M. Gutièrrez-Mecinas, J. P. Bolam & J. Boyes, unpublished observations). However, the precise localization of HCN channel subunits in relation to striatal cell types and afferents remains to be determined.

A second population of axon terminals also expressed presynaptic HCN channel subunits. These terminals formed asymmetric synapses with GP dendrites and were immunoreactive for VGLUT2, indicating that their probable origin is the STN, which provides the major glutamatergic input to the GP (Kita & Kitai, 1987; Smith *et al*., 1990b). When compared with inhibitory

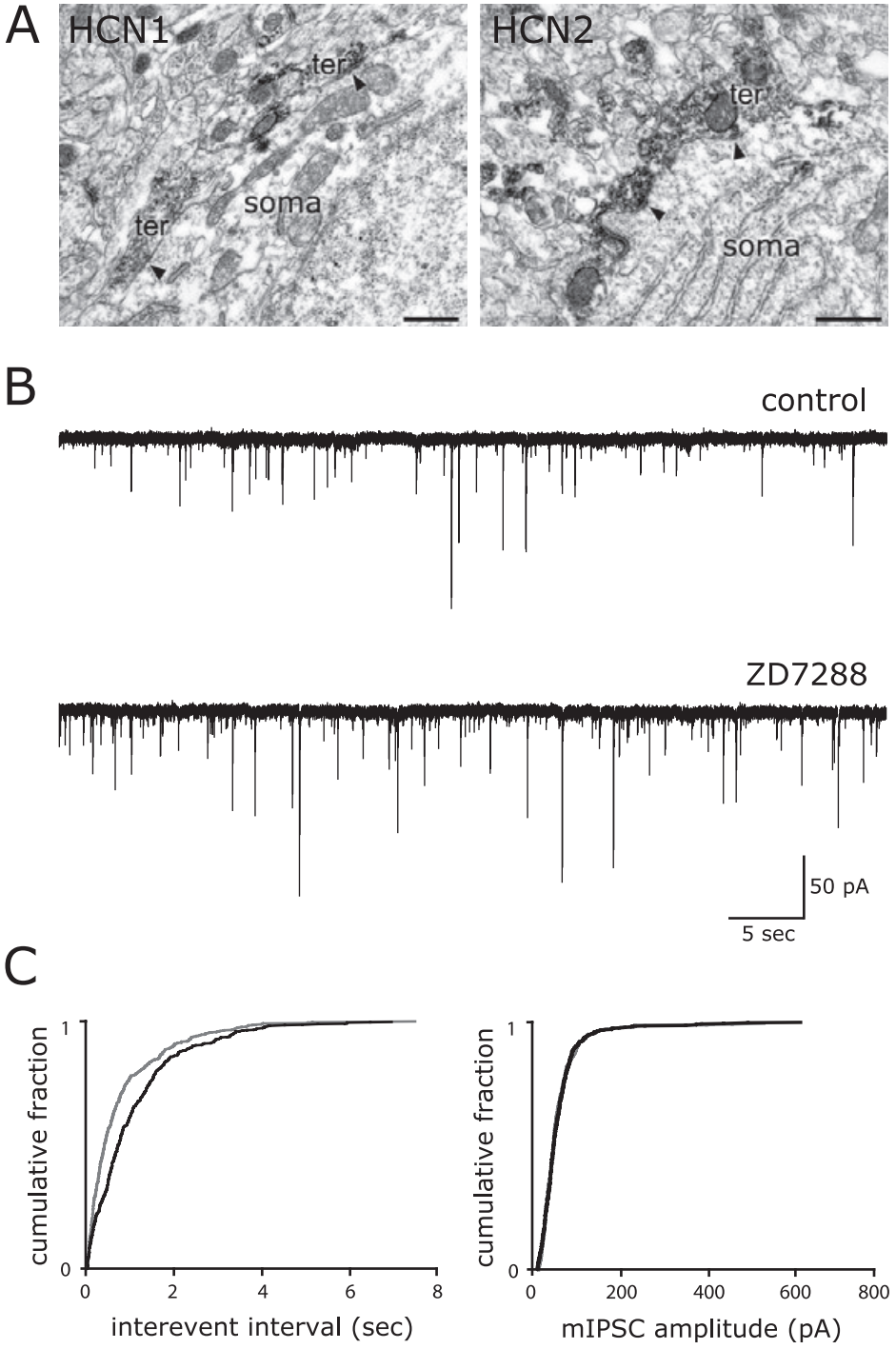

FIG. 7. ZD7288 increases the frequency of mIPSCs without affecting the amplitude. (A) Electron micrographs showing immunoperoxidase labelling for HCN1 (left) and HCN2 (right) in GP-like axon terminals at P14. (B) Voltage-clamp recordings of mIPSCs (recorded in the presence of TTX at −80 mV) under control conditions and 10 min after application of 50 μM ZD7288. (C) Cumulative interevent interval and amplitude distributions before and during ZD7288 application (black and grey lines, respectively). ZD7288 caused a significant shift towards shorter interevent intervals between mIPSCs ($P < 0.01$, Kolmogorov–Smirnov-test, $n = 5$), indicative of an increase in mIPSC frequency, but had no effect on the amplitude of mIPSCs. Scale bars in A, 0.5 μm.

terminals in the same tissue, labelling for HCN2 in glutamatergic terminals was considerably stronger than that for HCN1, consistent with the high level of HCN2 mRNA expression in the rodent STN (Monteggia *et al*., 2000; Santoro *et al*., 2000). The subunit composition of HCN channels is a major determinant of their activation properties, such that HCN1 channels activate more rapidly in response to membrane hyperpolarization than HCN2 channels, and at more positive potentials (Ludwig *et al*., 1998; Santoro *et al*., 1998). In the light of these differences, the predominant expression of HCN2 in STN terminals raises the possibility that these channels are functionally distinct from those located on the axon collaterals of GP neurons.

Presynaptic HCN channels regulate GABA release

In order to assess the role of presynaptic HCN channels in regulating inhibitory synaptic transmission in the GP, we used the HCN channel blocker ZD7288. ZD7288 has been shown to reduce the firing rate of GP neurons *in vitro* (Chan *et al*., 2004). Therefore, to eliminate the possible indirect effects of ZD7288 acting at HCN1/2 channels located on the soma and dendrites of other GP neurons in the slice, we recorded action-potential-independent mIPSCs in the presence of TTX. We observed a robust increase in the frequency of mIPSCs 10 min after the application of ZD7288, indicating that under basal conditions HCN channels regulate the release of GABA in the GP. Importantly, the time frame of the drug effect was similar to that reported previously (Harris & Constanti, 1995; Maccaferri & McBain, 1996; Gasparini & DiFrancesco, 1997; Svoboda & Lupica, 1998; Southan *et al*., 2000). Furthermore, this was markedly less than the time reported to lead to nonspecific changes in synaptic transmission in the hippocampus (Chevaleyre & Castillo, 2002). It is generally accepted that changes in the frequency of mIPSCs in response to a drug are indicative of a presynaptic locus of action. Thus, the effect of ZD7288 on mIPSCs is further support for our immunocytochemical data showing presynaptic HCN channels on inhibitory terminals in the GP. In our GP slice preparation, mIPSCs are presumed to originate from both pallidal and striatal terminals. However, our results suggest that striatopallidal terminals lack presynaptic HCN channel subunits. Thus, the action of ZD7288 on mIPSCs indicates that presynaptic HCN channels are involved in the modulation of GABA release from the recurrent axon collaterals of GP neurons.

The increase in the frequency of mIPSCs in response to ZD7288 contrasts with previous findings in the hippocampus, where similar concentrations of ZD7288 had little effect on mIPSC frequency (Lupica *et al*., 2001) or caused a decrease (Aponte *et al*., 2006). However, our results are similar to those of Southan *et al*. (2000), who reported a small increase in the frequency of mIPSCs recorded in cerebellar Purkinje cells. The reason for these different findings, and the mechanism by which HCN channels influence transmitter release, are unclear. Changes in the frequency of mIPSCs are likely to reflect a change in release probability. It is possible that blockade of HCN channels by ZD7288 hyperpolarizes the presynaptic terminals (away from the equilibrium potential for Ca^{2+}), thereby increasing the driving force for Ca^{2+} influx. The resulting elevation of the intraterminal Ca^{2+} concentration would be expected to enhance the probability of GABA release (Bouron, 2001). This hypothesis is dependent on the channels being active at the resting membrane potential of the terminals. In this regard, the contribution of a presynaptic HCN current has been demonstrated at the calyx of Held in the brainstem (Cuttle *et al*., 2001), where small deviations in resting potential have been shown to influence the probability of release in a Ca^{2+}-dependent manner (Awatramani *et al*., 2005). Another possibility is that presynaptic HCN channels interact directly with the transmitter release machinery, as has been suggested at the crayfish neuromuscular junction (Beaumont & Zucker, 2000). If this were the case, one might expect the channels to be clustered close to transmitter release sites in presynaptic terminals. In agreement with findings in other brain regions (Notomi & Shigemoto, 2004; Luján *et al*., 2005), however, immunogold labelling for HCN channel subunits in axon terminals was mostly localized at sites distant from the presynaptic active zone, suggesting a more generalized role for HCN channels in the regulation of presynaptic terminal excitability.

Postsynaptic HCN channels in the GP

Both HCN1 and HCN2 were localized in cell bodies and dendrites in the GP. Consistent with the presence of somatodendritic HCN channels, the majority of GP neurons respond to hyperpolarizing current steps with a time- and voltage-dependent depolarization, the hallmark of HCN channel activation (Cooper & Stanford, 2000; Chan *et al*., 2004). Our results further demonstrate that HCN1 and HCN2 are colocalized in subcellular compartments in the GP, including dendrites. This finding supports an earlier study showing coexpression of HCN1 and HCN2 mRNA in more than half of GABAergic GP neurons (Chan *et al*., 2004), and suggests that HCN1 and HCN2 may combine to form heteromeric channels, as has been demonstrated *in vitro* (Chen *et al*., 2001; Ulens & Tytgat, 2001). Indeed, hyperpolarization-activated currents recorded in GP neurons display both fast and slow components that are consistent with channels composed of HCN2 alone and HCN1–HCN2 heteromeric channels (Chan *et al*., 2004).

Functional implications

Our findings indicate that, in addition to the regulation of GP neuronal activity by HCN channels located at postsynaptic sites, the release of GABA by the local collaterals of GP neurons is under the regulation of presynaptic HCN channels. Our anatomical data further predict that HCN channels also play a role in the regulation of glutamate from STN terminals in the GP. The prominent expression of HCN2 channel subunits in both these populations of terminals has implications for the possible functions of the channels. In particular, channels containing the HCN2 subunit show greater activation by cyclic AMP than those containing only HCN1 (Ludwig *et al*., 1998; Santoro *et al*., 1998). As cyclic AMP is a known target of many modulators of presynaptic function, it is plausible that neuromodulators such as dopamine (Querejeta *et al*., 2001) exert their effects in the GP, at least in part, through an interaction with presynaptic HCN channels.

In common with other brains regions (Notomi & Shigemoto, 2004; Luján *et al*., 2005), we observed labelling for HCN1 and HCN2 in both myelinated and unmyelinated axons. A property of both GP and STN neurons is their ability to fire action potentials at high frequencies (> 100 Hz) for sustained periods (several seconds), and this is believed to be an essential feature of information processing in the basal ganglia. In many mammalian axons, prolonged stimulation at high frequencies causes the membrane to hyperpolarize (Grafe *et al*., 1997; Soleng *et al*., 2003). This hyperpolarization initiates an inward depolarizing current, resembling I_h, that helps to preserve the excitability and conduction reliability of these axons (Baker *et al*., 1987; Eng *et al*., 1990; Birch *et al*., 1991; Grafe *et al*., 1997; Soleng *et al*., 2003). Thus, axonal HCN channels may be important for ensuring faithful action potential propagation during periods of sustained activity.

Acknowledgements

This work was supported by the Medical Research Council, UK. We are grateful to Dr Andreas Ludwig for kindly providing the brains of $HCN2^{+/+}$ and $HCN2^{-/-}$ mice, Drs Peter Magill and Gavin Woodhall for helpful discussions and comments on the manuscript, and Liz Norman, Caroline Francis and Ben Micklem for excellent technical support.

Abbreviations

aCSF, artificial cerebrospinal fluid; GABA, γ-aminobutyric acid; GP, globus pallidus; HCN, hyperpolarization-activated, cyclic nucleotide-gated cation channel; I_h, hyperpolarization-activated cation current; mIPSC, miniature inhibitory postsynaptic current; P, postnatal day; STN, subthalamic nucleus; TTX, tetrodotoxin; VGLUT2, vesicular glutamate transporter 2.

References

Aponte, Y., Lien, C.C., Reisinger, E. & Jonas, P. (2006) Hyperpolarization-activated cation channels in fast-spiking interneurons of rat hippocampus. *J. Physiol. (Lond.)*, **574**, 229–243.

Awatramani, G.B., Price, G.D. & Trussell, L.O. (2005) Modulation of transmitter release by presynaptic resting potential and background calcium levels. *Neuron*, **48**, 109–121.

Baker, M., Bostock, H., Grafe, P. & Martius, P. (1987) Function and distribution of three types of rectifying channel in rat spinal root myelinated axons. *J. Physiol. (Lond.)*, **383**, 45–67.

Beaumont, V. & Zucker, R.S. (2000) Enhancement of synaptic transmission by cyclic AMP modulation of presynaptic I_h channels. *Nat. Neurosci.*, **3**, 133–141.

Bevan, M.D., Booth, P.A., Eaton, S.A. & Bolam, J.P. (1998) Selective innervation of neostriatal interneurons by a subclass of neuron in the globus pallidus of the rat. *J. Neurosci.*, **18**, 9438–9452.

Birch, B.D., Kocsis, J.D., Di Gregorio, F., Bhisitkul, R.B. & Waxman, S.G. (1991) A voltage- and time-dependent rectification in rat dorsal spinal root axons. *J. Neurophysiol.*, **66**, 719–728.

Bouron, A. (2001) Modulation of spontaneous quantal release of neurotransmitters in the hippocampus. *Prog. Neurobiol.*, **63**, 613–635.

Chan, C.S., Shigemoto, R., Mercer, J.N. & Surmeier, D.J. (2004) HCN2 and HCN1 channels govern the regularity of autonomous pacemaking and synaptic resetting in globus pallidus neurons. *J. Neurosci.*, **24**, 9921–9932.

Chan, C.S., Surmeier, D.J. & Yung, W.H. (2005) Striatal information signaling and integration in globus pallidus: timing matters. *Neurosignals*, **14**, 281–289.

Chen, L., Boyes, J., Yung, W.H. & Bolam, J.P. (2004) Subcellular localization of $GABA_B$ receptor subunits in rat globus pallidus. *J. Comp. Neurol.*, **474**, 340–352.

Chen, S., Wang, J. & Siegelbaum, S.A. (2001) Properties of hyperpolarization-activated pacemaker current defined by coassembly of HCN1 and HCN2 subunits and basal modulation by cyclic nucleotide. *J. Gen. Physiol.*, **117**, 491–504.

Chen, L. & Yung, W.H. (2004) GABAergic neurotransmission in globus pallidus and its involvement in neurologic disorders. *Sheng Li Xue Bao*, **56**, 427–435.

Chevaleyre, V. & Castillo, P.E. (2002) Assessing the role of I_h channels in synaptic transmission and mossy fiber LTP. *Proc. Natl Acad. Sci. USA*, **99**, 9538–9543.

Cooper, A.J. & Stanford, I.M. (2000) Electrophysiological and morphological characteristics of three subtypes of rat globus pallidus neurone in vitro. *J. Physiol. (Lond.)*, **527**, 291–304.

Cuttle, M.F., Rusznák, Z., Wong, A.Y., Owens, S. & Forsythe, I.D. (2001) Modulation of a presynaptic hyperpolarization-activated cationic current (I_h) at an excitatory synaptic terminal in the rat auditory brainstem. *J. Physiol. (Lond.)*, **534**, 733–744.

DeLong, M.R. (1971) Activity of pallidal neurons during movement. *J. Neurophysiol.*, **34**, 414–427.

Eng, D.L., Gordon, T.R., Kocsis, J.D. & Waxman, S.G. (1990) Current-clamp analysis of a time-dependent rectification in rat optic nerve. *J. Physiol. (Lond.)*, **421**, 185–202.

Filion, M. & Tremblay, L. (1991) Abnormal spontaneous activity of globus pallidus neurons in monkeys with MPTP-induced parkinsonism. *Brain Res.*, **547**, 142–151.

Fremeau, R.T. Jr, Voglmaier, S., Seal, R.P. & Edwards, R.H. (2004) VGLUTs define subsets of excitatory neurons and suggest novel roles for glutamate. *Trends Neurosci.*, **27**, 98–103.

Gasparini, S. & DiFrancesco, D. (1997) Action of the hyperpolarization-activated current (I_h) blocker ZD 7288 in hippocampal CA1 neurons. *Pflugers Arch.*, **435**, 99–106.

Grafe, P., Quasthoff, S., Grosskreutz, J. & Alzheimer, C. (1997) Function of the hyperpolarization-activated inward rectification in nonmyelinated peripheral rat and human axons. *J. Neurophysiol.*, **77**, 421–426.

Harris, N.C. & Constanti, A. (1995) Mechanism of block by ZD 7288 of the hyperpolarization-activated inward rectifying current in guinea pig substantia nigra neurons in vitro. *J. Neurophysiol.*, **74**, 2366–2378.

Jiang, Z.G. & North, R.A. (1991) Membrane properties and synaptic responses of rat striatal neurones in vitro. *J. Physiol. (Lond.)*, **443**, 533–553.

Kawaguchi, Y. (1993) Physiological, morphological, and histochemical characterization of three classes of interneurons in rat neostriatum. *J. Neurosci.*, **13**, 4908–4923.

Kita, H. (1994) Parvalbumin-immunopositive neurons in rat globus pallidus: a light and electron microscopic study. *Brain Res.*, **657**, 31–41.

Kita, H. & Kitai, S.T. (1987) Efferent projections of the subthalamic nucleus in the rat: light and electron microscopic analysis with the PHA-L method. *J. Comp. Neurol.*, **260**, 435–452.

Kita, H. & Kitai, S.T. (1991) Intracellular study of rat globus pallidus neurons: membrane properties and responses to neostriatal, subthalamic and nigral stimulation. *Brain Res.*, **564**, 296–305.

Kita, H. & Kitai, S.T. (1994) The morphology of globus pallidus projection neurons in the rat: an intracellular staining study. *Brain Res.*, **636**, 308–319.

Kita, H., Nambu, A., Kaneda, K., Tachibana, Y. & Takada, M. (2004) Role of ionotropic glutamatergic and GABAergic inputs on the firing activity of neurons in the external pallidum in awake monkeys. *J. Neurophysiol.*, **92**, 3069–3084.

Kita, H., Tokuno, H. & Nambu, A. (1999) Monkey globus pallidus external segment neurons projecting to the neostriatum. *Neuroreport*, **10**, 1467–1472.

Lacey, C.J., Boyes, J., Gerlach, O., Chen, L., Magill, P.J. & Bolam, J.P. (2005) $GABA_B$ receptors at glutamatergic synapses in the rat striatum. *Neuroscience*, **136**, 1083–1095.

Levy, R., Hazrati, L.N., Herrero, M.T., Vila, M., Hassani, O.K., Mouroux, M., Ruberg, M., Asensi, H., Agid, Y., Féger, J., Obeso, J.A., Parent, A. & Hirsch, E.C. (1997) Re-evaluation of the functional anatomy of the basal ganglia in normal and Parkinsonian states. *Neuroscience*, **76**, 335–343.

Lörincz, A., Notomi, T., Tamás, G., Shigemoto, R. & Nusser, Z. (2002) Polarized and compartment-dependent distribution of HCN1 in pyramidal cell dendrites. *Nat. Neurosci.*, **5**, 1185–1193.

Ludwig, A., Zong, X., Jeglitsch, M., Hofmann, F. & Biel, M. (1998) A family of hyperpolarization-activated mammalian cation channels. *Nature*, **393**, 587–591.

Luján, R., Albasanz, J.L., Shigemoto, R. & Juiz, J.M. (2005) Preferential localization of the hyperpolarization-activated cyclic nucleotide-gated cation channel subunit HCN1 in basket cell terminals of the rat cerebellum. *Eur. J. Neurosci.*, **21**, 2073–2082.

Lupica, C.R., Bell, J.A., Hoffman, A.F. & Watson, P.L. (2001) Contribution of the hyperpolarization-activated current (I_h) to membrane potential and GABA release in hippocampal interneurons. *J. Neurophysiol.*, **86**, 261–268.

Maccaferri, G. & McBain, C.J. (1996) The hyperpolarization-activated current (I_h) and its contribution to pacemaker activity in rat CA1 hippocampal stratum oriens-alveus interneurones. *J. Physiol. (Lond.)*, **497**, 119–130.

Magill, P.J., Bolam, J.P. & Bevan, M.D. (2000) Relationship of activity in the subthalamic nucleus-globus pallidus network to cortical electroencephalogram. *J. Neurosci.*, **20**, 820–833.

Monteggia, L.M., Eisch, A.J., Tang, M.D., Kaczmarek, L.K. & Nestler, E.J. (2000) Cloning and localization of the hyperpolarization-activated cyclic nucleotide-gated channel family in rat brain. *Brain Res. Mol. Brain Res.*, **81**, 129–139.

Nambu, A. & Llinás, R. (1997) Morphology of globus pallidus neurons: its correlation with electrophysiology in guinea pig brain slices. *J. Comp. Neurol.*, **377**, 85–94.

Notomi, T. & Shigemoto, R. (2004) Immunohistochemical localization of Ih channel subunits, HCN1-4, in the rat brain. *J. Comp. Neurol.*, **471**, 241–276.

Obeso, J.A., Rodriguez-Oroz, M.C., Javier Blesa, F. & Guridi, J. (2006) The globus pallidus pars externa and Parkinson's disease. Ready for prime time? *Exp. Neurol.*, **202**, 1–7.

Perkins, K.L. & Wong, R.K. (1995) Intracellular QX-314 blocks the hyperpolarization-activated inward current I_q in hippocampal CA1 pyramidal cells. *J. Neurophysiol.*, **73**, 911–915.

Querejeta, E., Delgado, A., Valsiosera, R., Erlij, D. & Aceves, J. (2001) Intrapallidal D_2 dopamine receptors control globus pallidus neuron activity in the rat. *Neurosci. Lett.*, **300**, 79–82.

Raz, A., Vaadia, E. & Bergman, H. (2000) Firing patterns and correlations of spontaneous discharge of pallidal neurons in the normal and the tremulous 1-methyl-4-phenyl-1,2,3,6-tetrahydropyridine vervet model of parkinsonism. *J. Neurosci.*, **20**, 8559–8571.

Robinson, R.B. & Siegelbaum, S.A. (2003) Hyperpolarization-activated cation currents: from molecules to physiological function. *Annu. Rev. Physiol.*, **65**, 453–480.

Sadek, A.R., Magill, P.J. & Bolam, J.P. (2005) Local connectivity between neurons of the rat globus pallidus. In Bolam, J.P., Ingham, C.A. & Magill, P.J. (eds), *The Basal Ganglia VIII*. Springer Science+Business Media, New York, pp. 611–619.

Santoro, B., Chen, S., Lüthi, A., Pavlidis, P., Shumyatsky, G.P., Tibbs, G.R. & Siegelbaum, S.A. (2000) Molecular and functional heterogeneity of hyperpolarization-activated pacemaker channels in the mouse CNS. *J. Neurosci.*, **20**, 5264–5275.

Santoro, B., Liu, D.T., Yao, H., Bartsch, D., Kandel, E.R., Siegelbaum, S.A. & Tibbs, G.R. (1998) Identification of a gene encoding a hyperpolarization-activated pacemaker channel of brain. *Cell*, **93**, 717–729.

Sato, F., Lavallee, P., Levesque, M. & Parent, A. (2000) Single-axon tracing study of neurons of the external segment of the globus pallidus in primate. *J. Comp. Neurol.*, **417**, 17–31.

Smith, Y., Bevan, M.D., Shink, E. & Bolam, J.P. (1998) Microcircuitry of the direct and indirect pathways of the basal ganglia. *Neuroscience*, **86**, 353–387.

Smith, Y., Bolam, J.P. & Von Krosigk, M. (1990a) Topographical and synaptic organization of the GABA-containing pallidosubthalamic projection in the rat. *Eur. J. Neurosci.*, **2**, 500–511.

Smith, Y., Hazrati, L.N. & Parent, A. (1990b) Efferent projections of the subthalamic nucleus in the squirrel monkey as studied by the PHA-L anterograde tracing method. *J. Comp. Neurol.*, **294**, 306–323.

Soleng, A.F., Chiu, K. & Raastad, M. (2003) Unmyelinated axons in the rat hippocampus hyperpolarize and activate an H current when spike frequency exceeds 1 Hz. *J. Physiol. (Lond.)*, **552**, 459–470.

Southan, A.P., Morris, N.P., Stephens, G.J. & Robertson, B. (2000) Hyperpolarization-activated currents in presynaptic terminals of mouse cerebellar basket cells. *J. Physiol. (Lond.)*, **526**, 91–97.

Stanford, I.M. (2003) Independent neuronal oscillators of the rat globus pallidus. *J. Neurophysiol.*, **89**, 1713–1717.

Svoboda, K.R. & Lupica, C.R. (1998) Opioid inhibition of hippocampal interneurons via modulation of potassium and hyperpolarization-activated cation (I_h) currents. *J. Neurosci.*, **18**, 7084–7098.

Terman, D., Rubin, J.E., Yew, A.C. & Wilson, C.J. (2002) Activity patterns in a model for the subthalamopallidal network of the basal ganglia. *J. Neurosci.*, **22**, 2963–2976.

Ulens, C. & Tytgat, J. (2001) Functional heteromerization of HCN1 and HCN2 pacemaker channels. *J. Biol. Chem.*, **276**, 6069–6072.